# Oscillations observed in Hydrocarbon Microtremor Analysis (HyMAS)


**R. HOLZNER , P. ESCHLE, M. LAMBERT and R. DEWARRAT, Spectraseis Technologie AG, Giessereistrasse 5, CH-8005 Zurich, Switzerland**
**P.F. MEIER, S.DANGEL, University of Zurich, Switzerland**
**R. GRAF, Proseis AG, Zurich, Switzerland**
**S. SCHMALHOLZ, B. STEINER AND M. FREHNER, Geological Institute, Swiss Federal Institute of Technology ETH Zurich, Switzerland**
**Y. PODLADCHIKOV, Physics of Geological Processes, University of Oslo, Norway**



## Abstract

Hydrocarbon Microtremor Analysis (HyMAS) is an innovative passive technology identifying the hydrocarbon content of geological structures by analyzing low frequency seismic signals. **Hydrocarbon indicating information** is extracted from spectral modifications of naturally occurring seismic background noise waves in the 0.01 – 10 Hz range passing through hydrocarbon bearing porous structures.

In this paper, a simple description of this reproducibly observable phenomenon in terms of a **one-dimensional linear model** of an oscillating liquid filled porous medium is presented and its relevance for an explanation of the underlying basic HyMAS signal creating mechanisms and related parameters are discussed. Observed values of about 3 Hz for the oscillation and $2 \cdot 10^{-6}$ m/s for the amplitude of the vertical surface movement velocity could be reproduced by introducing realistic parameter values for the geophysical properties in the model.

As a direct hydrocarbon indicator, HyMAS is an ideal complement to 2D- and 3D-seismic structural imaging technologies. Numerical modeling of suitable geological structures both in the macroscopic as well as in the microscopic domain shows how the seismic background noise spectrum can be modified in a different way when interacting with geological structures containing hydrocarbon filled pores compared to interacting with similar structures not containing hydrocarbons. In addition to reservoir detection, HyMAS also has the potental to determine reservoir parameter values and their evolution over time.


## HyMAS workflow

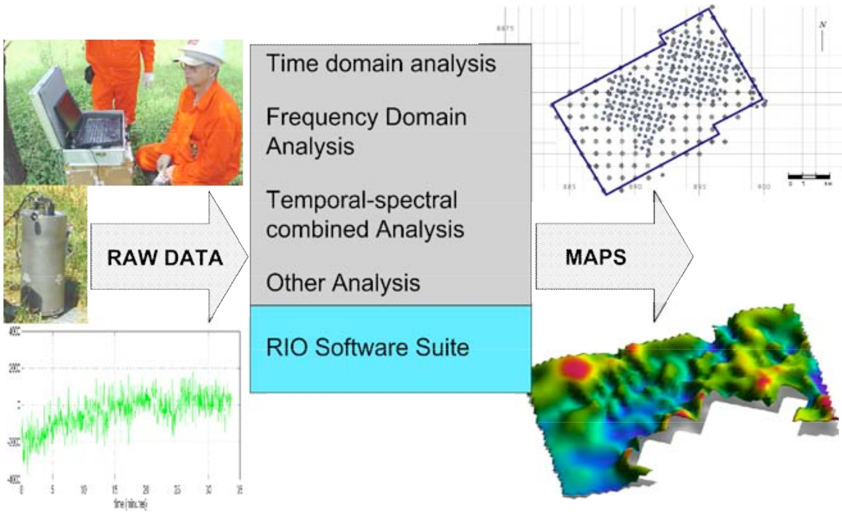


# Oscillations

Principle of HyMAS measurement: Background waves interacting with hydrocarbon bearing geological structures show spectral modifications, in this case around 3 Hz. The traces on top indicate typical spectral power densities of the vertical velocity component (HyMAS signal) measured outside (left) and directly above (right) a hydrocarbon reservoir.

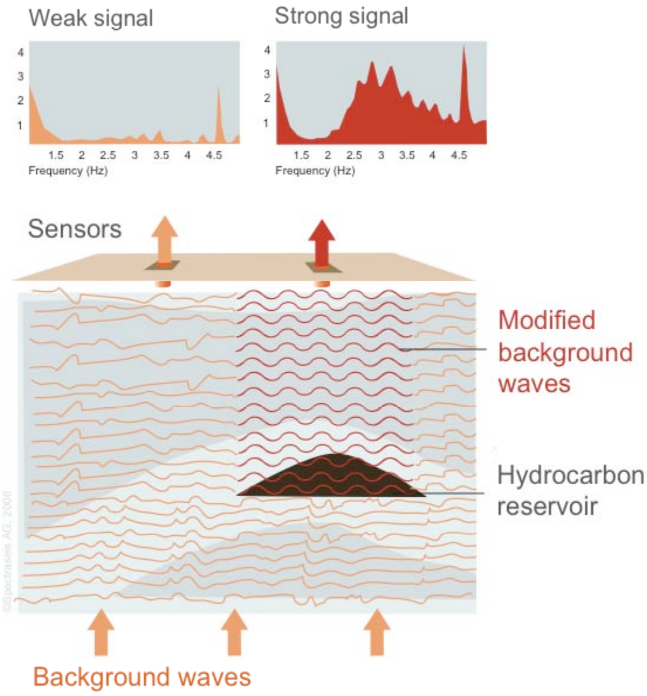


## linear harmonic oscillator model

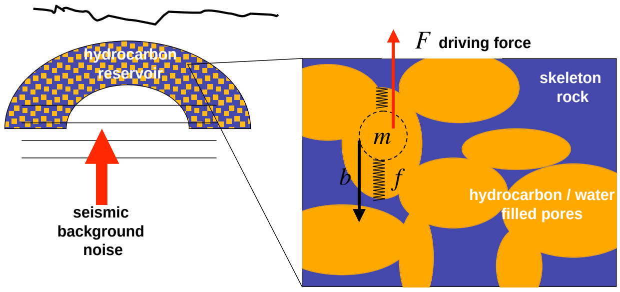


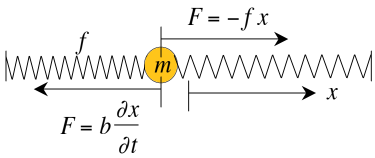


| | |
|---|---|
| $m$ | mass |
| $f$ | spring constant |
| $b$ | friction |
| $F_0$ | driving force |
| $\frac{b}{m}$ | damping |

$$\frac{\partial^2 x}{dt^2} + \frac{b}{m}\frac{\partial x}{dt} + \omega_0^2 x = \frac{F_0}{m}\cos(\omega t)$$

$$\omega_0 = \sqrt{\frac{f}{m}}$$ resonance frequency undamped

$$A(\omega) = \frac{F_0}{m} \cdot \frac{1}{\sqrt{\left(\omega^2 - \omega_0^2\right)^2 + \left(\frac{b}{m}\right)^2 \omega^2}}$$

$$\omega_{res} = \sqrt{\omega_0^2 - \frac{1}{2}\left(\frac{b}{m}\right)^2}$$ resonance frequency damped

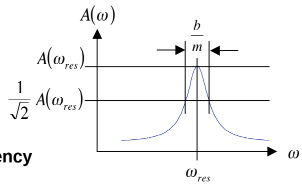


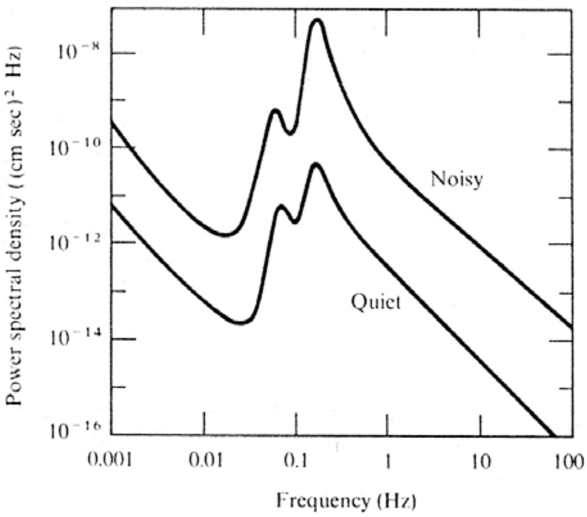


The main component of the ever present background wave field ( geological unrest) consists of the oceanic wave peaks around 0.1 Hz. They drive the hydrocarbon containing reservoir modelled as a one-dimensional harmonic oscillator which produces the wave pattern that can be detected at the surface by high sensitivity seismometers.

Aki, K., Richards, P.G.,
Quantitative seismology: theory and methods. Freeman 1980.


# Pores

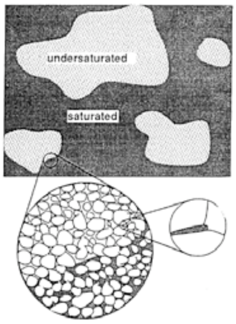


### "Patchy" saturation

The thinnest, compliant parts of the pore space
can be wetted throughout the rock,
but on much larger scales
some patches of the rock are
undersaturated while other patches
are fully saturated.

From Mavko & Nolen-Hoeksema
1994 in
X. Li et al " PHYSICS OF PARTIALLY
SATURATED POROUS MEDIA: Residual
Saturation and Seismic-Wave Propagation"
Annu. Rev. Earth. Planet. Sci. 29(2001)419-460.
050809hre1646

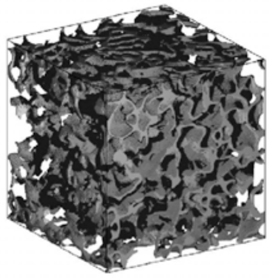

### "Digital rock" sample

An open-cell Gaussian random field (GRF3).
The structure shown is the porespace, the
transparent part is the grain material.

E. H. Saenger and S. A. Shapiro " Seismic
effects of viscous Biot-coupling: Finite difference
simulations on micro-scale"
Geophys. Res. Let. 32, L14310 (2005)1-5.
050809hre1700

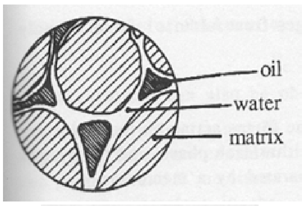


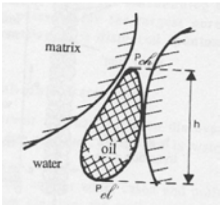


### "Capillary Migration"

R. Cossé " Basics of Reservoir Engineering"
Editions Technip, Paris (1993)

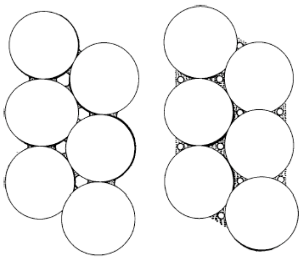

### "pendular" and "funicular" saturation

For a fluid phase in the pendular regime, the
fluid is immobilized by capillary
trapping.

The funicular regime of saturation occurs when
the porous medium has an intermediate
saturation with both phases. Funicular liquid
bodies touch each other and merge, forming a
continuous network of both phases in the
porous medium.

From Scheidegger 1974 in
X. Li et al " PHYSICS OF PARTIALLY
SATURATED POROUS MEDIA: Residual
Saturation and Seismic-Wave Propagation"
Annu. Rev. Earth. Planet. Sci. 29(2001)419-460.
050809hre1646

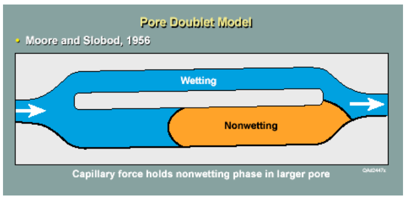


### Non-wetting pores

M.H. Holtz
"Development of a $CO_2$ sequestration"
as a residual phase in brine-saturated
formations"

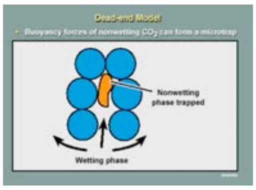


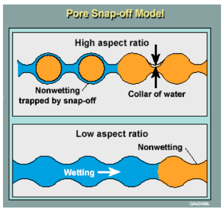


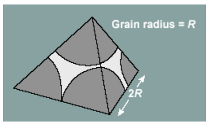


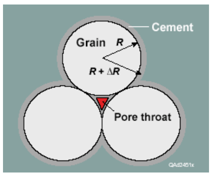


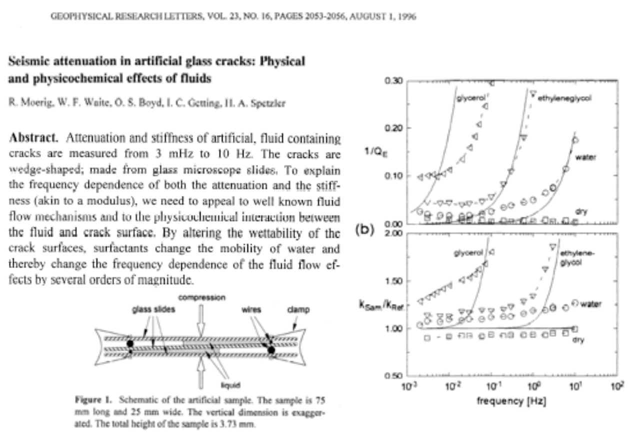

GEOPHYSICAL RESEARCH LETTERS, VOL. 23, NO. 16, PAGES 2053-2056, AUGUST 1, 1996

**Seismic attenuation in artificial glass cracks: Physical and physicochemical effects of fluids**

R. Moerig, W. F. Waite, O. S. Boyd, I. C. Getting, H. A. Spetzler

**Abstract.** Attenuation and stiffness of artificial, fluid containing cracks are measured from 3 mHz to 10 Hz. The cracks are wedge-shaped; made from glass microscope slides. To explain the frequency dependence of both the attenuation and the stiffness (akin to a modulus), we need to appeal to well known fluid flow mechanisms and to the physicochemical interaction between the fluid and crack surface. By altering the wettability of the crack surfaces, surfactants change the mobility of water and thereby change the frequency dependence of the fluid flow effects by several orders of magnitude.



**Figure 1.** Schematic of the artificial sample. The sample is 75 mm long and 25 mm wide. The vertical dimension is exaggerated. The total height of the sample is 3.73 mm.

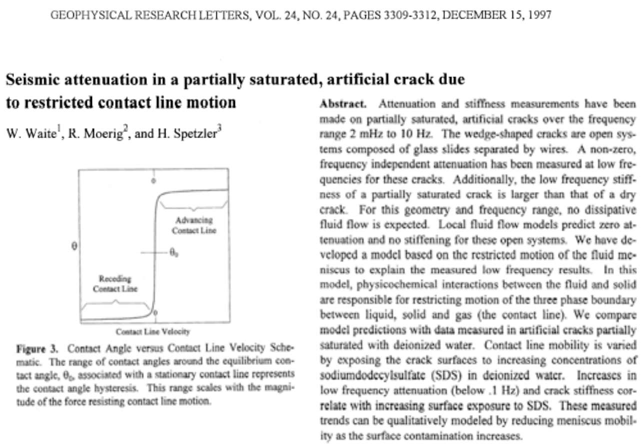

GEOPHYSICAL RESEARCH LETTERS, VOL. 24, NO. 24, PAGES 3309-3312, DECEMBER 15, 1997

**Seismic attenuation in a partially saturated, artificial crack due to restricted contact line motion**

W. Waite[1], R. Moerig[2], and H. Spetzler[3]



**Figure 3.** Contact Angle versus Contact Line Velocity Schematic. The range of contact angles around the equilibrium contact angle, $\theta_0$, associated with a stationary contact line represents the contact angle hysteresis. This range scales with the magnitude of the force resisting contact line motion.

**Abstract.** Attenuation and stiffness measurements have been made on partially saturated, artificial cracks over the frequency range 2 mHz to 10 Hz. The wedge-shaped cracks are open systems composed of glass slides separated by wires. A non-zero, frequency independent attenuation has been measured at low frequencies for these cracks. Additionally, the low frequency stiffness of a partially saturated crack is larger than that of a dry crack. For this geometry and frequency range, no dissipative fluid flow is expected. Local fluid flow models predict zero attenuation and no stiffening for these open systems. We have developed a model based on the restricted motion of the fluid meniscus to explain the measured low frequency results. In this model, physicochemical interactions between the fluid and solid are responsible for restricting motion of the three phase boundary between liquid, solid and gas (the contact line). We compare model predictions with data measured in artificial cracks partially saturated with deionized water. Contact line mobility is varied by exposing the crack surfaces to increasing concentrations of sodiumdodecylsulfate (SDS) in deionized water. Increases in low frequency attenuation (below .1 Hz) and crack stiffness correlate with increasing surface exposure to SDS. These measured trends can be qualitatively modeled by reducing meniscus mobility as the surface contamination increases.

# Micromechanical Models

$$\omega_{res} = \sqrt{\omega_0^2 - 2\rho^2} = \sqrt{\frac{f^2}{m^2} - \frac{b^2}{2m^2}} = \frac{1}{m}\sqrt{f^2 - \frac{1}{2}b^2}$$

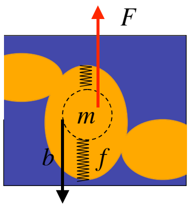


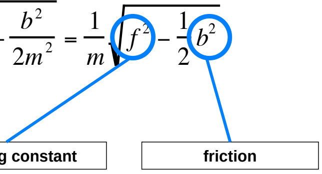


**spring constant** — **surface tension**, **gas content**

**friction** — **viscosity**

**porosity**
**permeability**
**temperature**
**pressure**

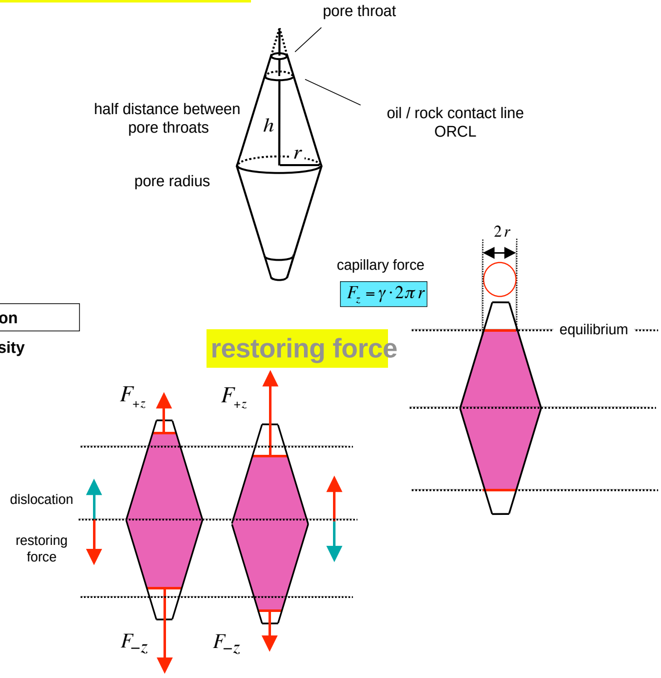


Bi-conical pore geometry which enables low frequency oscillations of the contained liquid along the z-direction. The liquid surface boundary forms the oil/rock contact line (ORCL) between the oil and water phases as well as the water wetted pore surface where capillary forces occur. Liquid in equilibrium: the capillary forces in positive and in negative z direction balance each other. After a small displacement of the liquid in the positive z-direction the capillary force pointing upward has decreased and the one pointing downward has increased compared to the equilibrium. The resulting restoring force drives the liquid back along the negative z-direction towards its equilibrium position. The same holds for a dislocation in the negative z-direction.

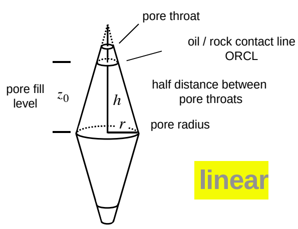


$$\frac{b}{m} = \frac{\sqrt{6}\cdot\eta\cdot z_0}{\pi\, r^2 (h - z_0)\,\rho_L}$$

$2\rho = \frac{b}{m}$ **Damping**

$\omega_{res} = \sqrt{\omega_0^2 - 2\rho^2}$ **resonance frequency damped**

**linear**

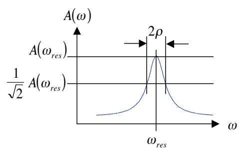


Spherical pore geometry which enables low frequency oscillations of the contained liquid along the z-direction.

**nonlinear**

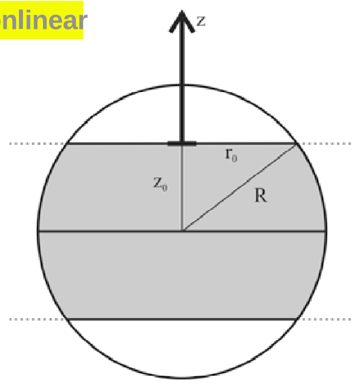


linear spring constant $f = \frac{\partial F_z}{\partial z} = \gamma \frac{2\pi r}{h}$

oscillating mass $m = \frac{2}{3} r^2 \pi\, h\, \rho_L$

restoring capillary force $F_z = \gamma \cdot 2\pi r$

resonance frequency $\nu = \frac{1}{2\pi}\sqrt{\frac{f}{m}} = \frac{1}{2\pi h}\sqrt{\frac{6\gamma}{r\,\rho_L}}$

While the bi-conical pore geometry leads to a linear spring constant for the restoring motion, the spherical pore geometry results in a non-linear spring constant that depends on the dislocation.

$$m = \frac{4}{3}\pi r^3 \rho_L \frac{\left(3r^2 z_0 - z_0^3\right)}{2r^3}$$

$$f = \frac{\partial}{\partial z}\left(\gamma 2\pi r(z)\right) = 2\pi\gamma \frac{\partial}{\partial z}\sqrt{r^2 - (z_0 + z)^2} = -\frac{2\pi\gamma (z_0 + z)}{\sqrt{r^2 - (z_0 + z)^2}}$$

$$\omega_0 = \sqrt{f/m} \approx \sqrt{\frac{2\pi\gamma z_0}{m\sqrt{r^2 - z_0^2}}}$$


# Comparison of measured and modelled spectra

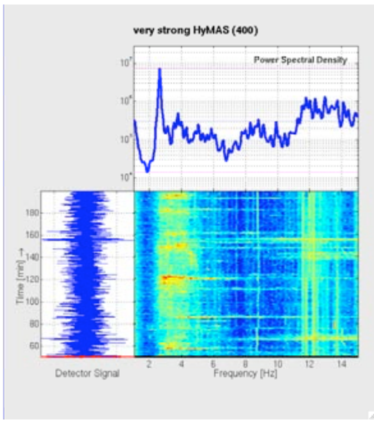


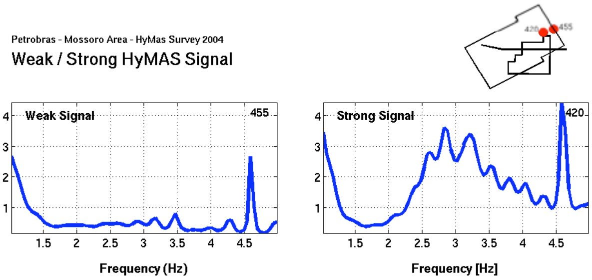


**field measurements**

Numerical simulation of the superimposed spectrum of 1000 linear harmonic oscillators for three different parameter distributions:

a) all oscillators with normalized resonance frequency at $\omega_0 = 1$ and damping $\rho = 0.1$ ;

b) both resonance frequency and damping vary according to a log-normal distribution with sigma = 2.84;

c) both resonance frequency and damping vary according to a broad log-normal distribution with sigma = 3.47.

**average over many oscillators**

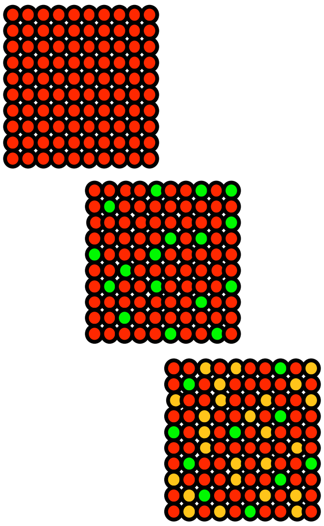

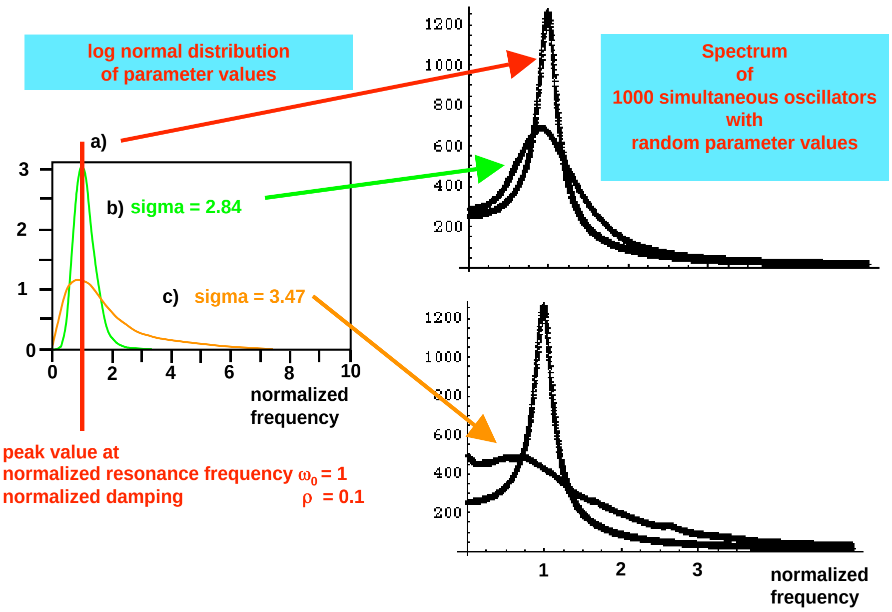


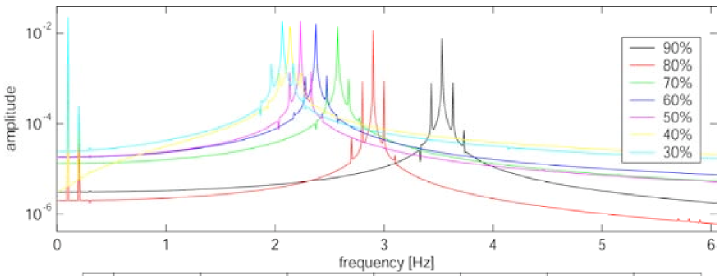


Spectrum of nonlinear oscillations in a spherical pore for different filling levels between between 0.3 and 0.9 of the pore liquid. The frequency spacing of the multiple peaks is a typical feature of nonlinear systems and corresponds to the frequency of the driving oscillation at 0.1 Hz, which also produces its own overtone at 0.2 Hz. For demonstration reasons, the damping was set to zero which leads to sharper peaks.

**nonlinear response**

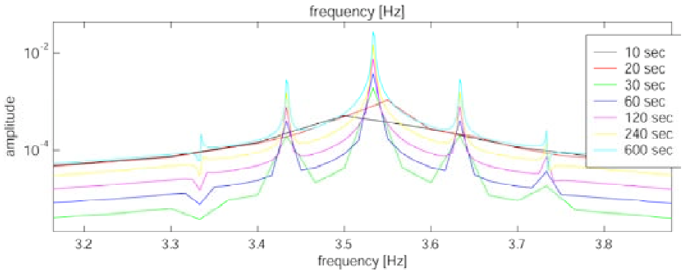


Development of the spectrum of nonlinear oscillations in a spherical pore during 600 s for filling level = 0.9 of the pore liquid. The frequency spacing of the multiple peaks is a typical feature of nonlinear systems and corresponds to the frequency of the driving oscillation at 0.1 Hz.

Natural oscillation frequency of pore: n =3.527 Hz, mass of liquid in pore m = 2.64 ·10-5 kg.


# Macroscopic modelling

The micromechanical motion of the pore content transmits some of its energy to the surrounding rock material by friction. The resulting collective effect averaged over the pores containing hydrocarbons can be measured at the surface as seismic vibrations or microtremors. The analysis by the one-dimensional oscillator scheme allows for a convenient approximation both for the observed frequency as well as for the vibration strength. For an adequate numerical model in 2D or 3D, a more sophisticated approach has to be used which involves the integration of effects on the pore scale into a macroscopic system of calculation grid points.

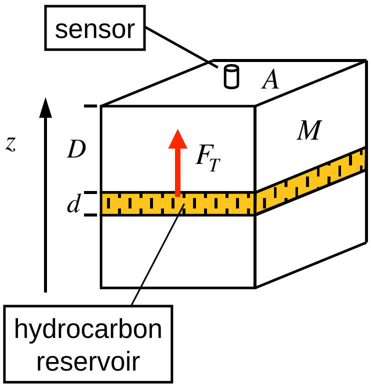


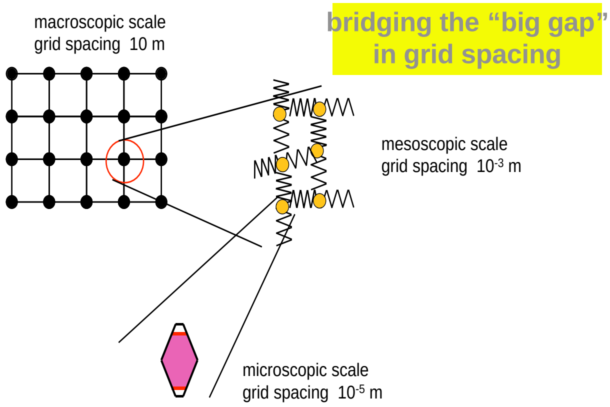


$n \cdot V_p = \eta \cdot V,$

$n$ : number of pores in reservoir,

$V_p$ : pore volume,

$\eta$ : porosity,

$V$ : reservoir volume

$$n \cdot 2 \cdot \frac{1}{3} r^2 \pi h = \eta \cdot d \cdot A$$

$$n = \frac{3 \eta d A}{2 r^2 \pi h}$$

$$F_T = M \frac{\partial^2 z}{\partial t^2}$$

$F_T$ : total frictional force in reservoir,

$M$ : total mass above reservoir,

$$\frac{\partial z}{\partial t} = \int \frac{F_T}{M} \partial t = -\frac{n \cdot c \cdot \gamma \cdot 2\pi r \cos(\omega t)}{M\omega} = -\frac{\frac{3 \eta d A}{2 r^2 \pi h} c \cdot \gamma \cdot 2\pi r}{A \cdot D \cdot \rho_R \cdot \omega} \cos(\omega t) = -\frac{3 \eta d c \gamma}{D \rho_R r h \omega} \cos(\omega t) = -v_z \cos(\omega t)$$

$F_z = c \cdot \gamma \cdot 2\pi r \sin(\omega t)$ **frictional force in pore**

$F_T = n F_z$ **total frictional force in reservoir**

$n = \frac{3 \eta d A}{2 r^2 \pi h}$ **number of pores**

$F_T = M \frac{\partial^2 z}{\partial t^2}$ **Newton's equation of motion**

**measured velocity of earth motion**

$$v_z = \frac{3 \eta d c \gamma}{r h \omega D \rho_R}$$

see also
**Poster P13 :**
M. Lambert et al.
*"Using low-frequency ambient seismic vibration spectra to detect hydrocarbon reservoirs – a numerical approach"*

# Identification of reservoir parameters

The interaction of background waves with a hydrocarbon bearing reservoir generates characteristic wave patterns which depend on the specific parameters of the reservoir such as density, porosity, permeability, saturation, interfacial tension between the liquids and gases contained in the pore and geometry of the reservoir. Approximated values of these parameters can be predicted by comparison of synthetic signals generated by the numerical model and real data acquired over the survey field.

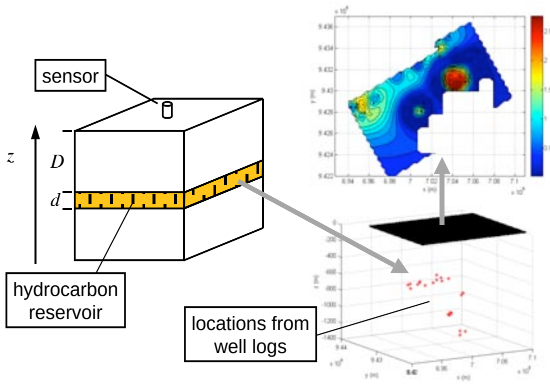


resonance frequency

$$\omega = \frac{1}{h} \sqrt{\frac{6\gamma}{r \rho_L}}$$

measured velocity of earth motion

$$v_z = \frac{3 \eta d c \gamma}{r h \omega D \rho_R}$$

| | | | |
|---|---|---|---|
| surface tension of oil | $\gamma = 10^{-3} \frac{\text{N}}{\text{m}}$ | depth of hydrocarbon containing formation | $D = 10^3 \text{m}$ |
| density of oil | $\rho_L = 8 \cdot 10^2 \frac{\text{kg}}{\text{m}^3}$ | hydrocarbon layer thickness | $d = 20\text{m}$ |
| pore radius | $r = 10^{-3} \text{m}$ | porosity | $\eta = 0.2$ |
| half distance between pore throats | $h = 5 \cdot 10^{-3} \text{m}$ | density of rock material | $\rho_R = 2 \cdot 10^3 \frac{\text{kg}}{\text{m}^3}$ |
| | | fraction of maximum capillary force at ORCL=$2\pi r$ | $c = 10^{-2}$ |
| resonance frequency | $\omega = 2\pi \cdot 3\text{Hz}$ | velocity of surface motion | $v_z = 2 \cdot 10^{-6} \frac{\text{m}}{\text{s}}$ |